Advanced Powder Technology 24 (2013) 86–92

Contents lists available at SciVerse ScienceDirect

Advanced Powder Technology

journal homepage: www.elsevier.com/locate/apt

Original Research Paper

Mechanochemical synthesis of a $La_{0.67}Ce_{0.21}Nd_{0.08}Pr_{0.04}Ni_5$ intermetallic compound

V. Blanco [a,b], M.R. Esquivel [a,c,d,*]

[a] Comisión Nacional de Energía Atómica (CNEA), Centro Atómico Bariloche, Av. Bustillo km 9.5 (R8402AGP), S.C. de Bariloche, Argentina
[b] Instituto Balseiro, Universidad Nacional de Cuyo (UNCo) y (CNEA), Argentina
[c] Consejo Nacional de Investigaciones Científicas y Técnicas, Argentina
[d] Centro Regional Universitario Bariloche, (UNCo), Quintral 1250, (R8400FRF), S.C. de Bariloche, Argentina

ARTICLE INFO

Article history:
Received 16 February 2011
Received in revised form 13 January 2012
Accepted 19 February 2012
Available online 3 March 2012

Keywords:
XRD
Powder metallurgy
Mechanical alloying
Mechanical milling

ABSTRACT

The mechanochemical synthesis of a $La_{0.67}Ce_{0.21}Nd_{0.08}Pr_{0.04}Ni_5$ intermetallic is studied. The intermetallic is synthesised from a mixture of $LaNi_5$ and $La_{0.25}Ce_{0.52}Nd_{0.17}Pr_{0.06}Ni_5$. The processes controlling the mechanical alloying are characterised as a function of integrated milling time (t_m). Effects of fracture and cold welding on the sample are identified by scanning electron microscopy. Compositional, microstructural and structural changes are analysed by energy dispersive spectroscopy and X-ray diffraction. The powder obtained has a particle size distribution of 9 ± 1 μm with an average crystallite size of 370 ± 10 Å and strain >10%. The intermetallic compound is annealed in Ar to increase crystallite size and to release strain. The structure is refined by the Rietveld method. Cell parameters are a = 4.982(2) Å and c = 3.980(9) Å, respectively. The advantage of the synthesis method using intermetallics instead of metals/alloys is discussed along with the characteristics of the powder obtained.

1. Introduction

Multi-substituted AB_5 intermetallics are used in different applications of the hydrogen technology such as hydrogen compression, static hydrogen storage and rechargeable batteries [1–3]. These intermetallics can be obtained by mechanical alloying of metals/alloys constituents [4–6]. Intermetallics are obtained as powders which make the handling easier and cheaper.

In these intermetallics, A represents a lanthanide ad B represents a metal of the groups 3–11. The A-type element is usually more ductile than the B-type element. Usually the A-type metal is laminated preferentially on the milling chamber and the final AB_5 is not stoichiometric [4]. This issue can be overcome by using mixtures of intermetallics instead of mixtures of metals. The intermetallics have similar ductility and no preferential lamination of the lanthanide might occur. But the milling of intermetallics is not studied. Therefore, the processes governing the evolution of the powders during mechanical alloying need to be characterised. This study should be done to optimise the integrated milling time (t_m), the amount of energy used and the final characteristics of the powder.

In this work, a mixture of intermetallics of the AB_5-type was mechanically alloyed to synthesise a new intermetallic compound of composition $La_{0.67}Ce_{0.21}Nd_{0.08}Pr_{0.04}Ni_5$.

The evolution of the powder morphology, microstructure and composition was analysed. The characterisation of the stages of mechanical alloying was studied. The processing parameters were identified and quantified. The materials obtained will be used in the development of a multistage hydrogen compression system. This objective aimed the elaboration of this work.

2. Experimental

$La_{0.25}Ce_{0.52}Nd_{0.17}Pr_{0.06}$ (99.7%, Alpha Aesar) and Ni powder (99.999%, Sigma–Aldrich) were used as raw materials. The mixture was mechanically alloyed during 200 h in a low-energy ball mill (Uni-Ball-Mill II, Australian Scientific Instruments). The mixture was processed in a stainless steel container under Ar atmosphere. A 120 rpm milling speed was selected. Stainless steel balls/sample mass ratio was 22.1. Neutron Activation Analysis (NAA) was performed in order to verify lanthanide alloy composition. A mixture containing 40% mass of the resulting intermetallic, $La_{0.25}Ce_{0.52}Nd_{0.17}Pr_{0.06}Ni_5$ and 60% mass of $LaNi_5$ (99.9%) was processed for 405 min in a middle energy ball mill (Pulverissette 6, Fritsch). A constant ball/sample mass ratio (6.28) was maintained. Milling speeding selected was 100 rpm. All handlings were carried out in a glove box (Plas and Labs). Oxygen level was monitored by a trace analyser (Series 3000, Alpha Omega) and it was kept under 20 ppm.

In order to characterise the different stages of mechanical alloying, samples representative of different t_m were examined.

* Corresponding author at: Comisión Nacional de Energía Atómica (CNEA), Centro Atómico Bariloche, Av. Bustillo km 9.5 (R8402AGP), S.C. de Bariloche, Argentina. Tel.: +54 02944 445156; fax: +54 02944 445290.
E-mail address: esquivel@cab.cnea.gov.ar (M.R. Esquivel).

0921-8831/$ - see front matter © 2012 The Society of Powder Technology Japan. Published by Elsevier B.V. and The Society of Powder Technology Japan. All rights reserved.
doi:10.1016/j.apt.2012.02.005

Annealing treatment (600 °C, during 24 h under Ar atmosphere) was performed to final samples. Particle size distribution and morphology were observed by Scanning Electron Microscopy (SEM 515, Philips Electronic Instruments). Particle size distribution was done by immersion of an aliquot of the sample on n-isobutilic alcohol followed by set of the sample on ultrasound and dropping part of the suspension on the SEM holder. Images were taken at the higher contrast and binarised (black and white). Particle analysis was done with ITEM software©. Intermetallics composition was determined by energy dispersive spectroscopy (EDS). Structural and microstructural parameters were established by room temperature X-ray Diffraction (Philips diffractometer, PW 1710/01, Cu Kα radiation and graphite monochromator). Crystalline Si was used as reference pattern. The phases were refined by Rietveld method using DBWS software [7]. Strain and crystallite size were estimated from diffraction peaks by assuming empirically a Gauss distribution and a Cauchy (Lorentz) component, respectively. Thermal stability of the compounds was studied by Differential Scanning Calorimetry (DSC TA 2910 calorimeter). The heating runs were performed under 122 mL min^{-1} in Ar flow. Heating rate selected was 5 °C min^{-1}, from room temperature to 570 °C.

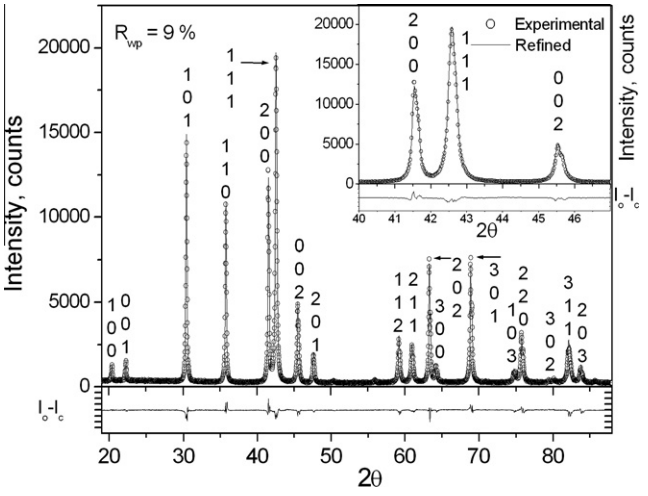

Fig. 1. Diffractogram of starting $LaNi_5$. Bottom: difference between observed (I_o) and calculated (I_c) intensities. Inset: detail of the refinement.

3. Results and discussion

3.1. Characterisation of $LaNi_5$ and $La_{0.25}Ce_{0.52}Nd_{0.17}Pr_{0.06}Ni_5$

The diffractogram of starting $LaNi_5$ is presented in Fig. 1. The hkl diffraction planes are indicated in the figure and the structure was refined by the Rietveld method [8]. The experimental (hollow dots) and calculated (black line) values are also presented in the upper inset of Fig. 1. The lower part of the figure and inset shows the difference between observed (I_o) and calculated (I_c) intensities. As observed, no phase other than the AB_5 is present in the sample. A summary of the obtained parameters is presented in Table 1. The R_{wp} value stands for the goodness of the fit.

The $LaNi_5$ profile shows well defined peaks indicating a large crystalline degree along with the low values of strain. These micro structural parameters are calculated for three hkl family planes. The values are shown in Table 2.

The diffractogram of starting $La_{0.25}Ce_{0.52}Nd_{0.17}P_{r0.06}Ni_5$ is presented in Fig. 2. The structure was also refined by the Rietveld method. The observed (I_o) and calculated (I_c) intensities are presented at the bottom and inset of Fig. 2. The sample presents other phases: Ni and $(La_{0.25}Ce_{0.52}Nd_{0.17}Pr_{0.06})_2Ni_7$. Ni peaks are identified with full circles. $(La_{0.25}Ce_{0.52}Nd_{0.17}Pr_{0.06})_2Ni_7$ peaks are indicated with full squares. Phases were refined and quantified using the Rietveld method. Hexagonal $(La_{0.25}Ce_{0.52}Nd_{0.17}Pr_{0.06})_2Ni_7$ structure was refined using the structural data of homologous La_2Ni_7 [9]. The

Table 1
Structural parameters of the AB_5 intermetallics obtained using the Rietveld method. R_{wp} stands for the goodness of the fit. M stands for lanthanide ($La_{0.25}Ce_{0.52}Nd_{0.17}Pr_{0.06}$) composition. M′ stands for lanthanide ($La_{0.67}Ce_{0.21}Nd_{0.08}Pr_{0.04}$) composition. S.G is space group. F.U is formula unit. Wy and x,y,z represent the Wyckoff and the coordinates of the position, respectively.

Sample	Compound S.G F.U	Cell parameters			Atomic positions			Mass%	R_{wp}
		a (Å) b (Å)	c (Å)	α β γ	At	Wy	(x,y,z)		
Starting $LaNi_5$	$LaNi_5$ $P6/mmm$ 1	5.017(0)	3.981(7)	90 90 120	La Ni Ni	1a 2c 3g	(0,0,0) (1/3,2/3,0) (1/2,0,1/2)	100	9
Starting MNi_5	MNi_5 $P6/mmm$ 1	4.927(6)	3.998(4)	90 90 120	M Ni Ni	1a 2c 3g	(0,0,0) (1/3,2/3,0) (1/2,0,1/2)	82 ± 2	10
	Ni $Fm3m$ 4	3.543(2)		90 90 90	Ni	4a	(0,0,0)	16 ± 3	
	M_2Ni_7 $P6_3/mmc$ 4	5.001(4)	7.235(1)	 90 90 120	M M Ni Ni Ni Ni Ni	4f 4f 2a 4e 4f 6h 12k	(1/3,2/3,0.03) (1/3,2/3,0.1750) (0,0,0) (0,0,0.167) (1/3,2/3,0.833) (0.835,0.670,1/4) (0.834,0.688,0.085)	~3	
Obtained $M'Ni_5$	$M'Ni_5$ $P6/mmm$ 1	4.982(2)	3.980(9)	90 90 120	La Ni Ni	1a 2c 3g	(0,0,0) (1/3,2/3,0) (1/2,0,1/2)	72 ± 2	10
	Ni $Fm3m$ 4	3.536(0)		90 90 90	Ni	4a	(0,0,0)	28 ± 1	
	M'_2Ni_3 $Cmca$ 4	5.278(2) 9.529(5)	7.771(3)	90 90 90	La Ni Ni	8f 8e 4a	(1/2,0.1563,0.0904) (0.25,0.419,0.25) (0,0,0)	~2	

Table 2
Microstructural parameters of AB_5 compounds obtained by XRD.

Sample	Treatment	hkl	$d \pm 10$ (Å)	s (%)
$LaNi_5$	Starting	101	1400	2
		110	1750	1
		111	1000	2
$La_{0.25}Ce_{0.52}Nd_{0.17}Pr_{0.06}Ni_5$	Starting	101	410	7
		110	530	5
		111	290	4
$La_{0.67}Ce_{0.21}Nd_{0.08}Pr_{0.04}Ni_5$	As-milled	101	290	>10
		110	420	>10
		111	290	>10
$La_{0.67}Ce_{0.21}Nd_{0.08}Pr_{0.04}Ni_5$	As-milled + annealed	101	1440	>7
		110	1120	>7
		111	1180	>7

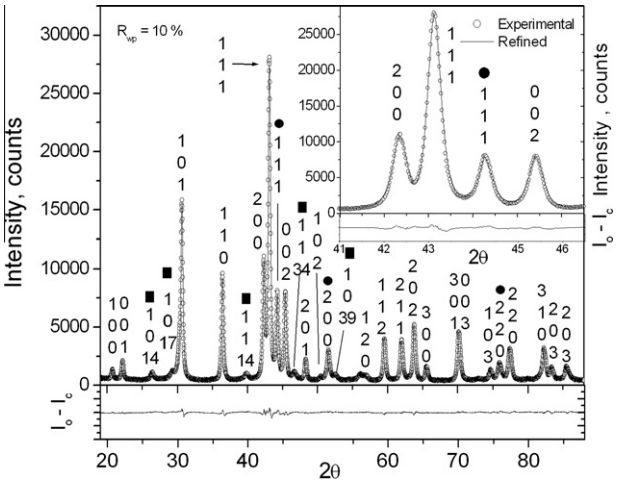

Fig. 2. Diffractogram of starting $La_{0.25}Ce_{0.52}Nd_{0.17}Pr_{0.06}Ni_5$ bottom: difference between observed (I_o) and calculated (I_c) intensities. Ni peaks are indicated with full circles. $(La_{0.25}Ce_{0.52}Nd_{0.17}Pr_{0.06})_2Ni_7$ peaks are indicated with full squares. Inset: detail of the refinement.

chemical composition of these phases was obtained by EDS. Results are summarised in Table 1. Then, the mechanical alloying of the starting $La_{0.25}Ce_{0.52}Nd_{0.17}Pr_{0.06}$ + 5Ni leads to the formation of $MNi_5 + M_2Ni_7$ + Ni, where M stands for $La_{0.25}Ce_{0.52}Nd_{0.17}Pr_{0.06}$ composition. As observed in Table 1, M_2Ni_7 is the minor one.

The profile shows a well crystallised sample. Both strain and crystallite sizes were also quantified for three hkl family planes of the AB_5 phase. The results are summarised in Table 2. As observed, crystallite sizes are smaller than those of $LaNi_5$. The strain values are larger than those of $LaNi_5$. This occurs because of the synthesis method as reported in experimental section. As indicated, $La_{0.25}Ce_{0.52}Nd_{0.17}Pr_{0.06}Ni_5$ is obtained by mechanical alloying followed by annealing at 600 °C during 24 h. Unlike the $LaNi_5$ sample annealed at high temperatures (T = 950 °C), the structure possess smaller crystalline domains and larger strain values.

For comparison, the cell parameters reference of AB_5 structures is presented: $LaNi_5$ (PDF-653777; a = 4.926 Å; c = 4.008 Å), $CeNi_5$ (PDF-653463; a = 4.874 Å; c = 4.004 Å), $NdNi_5$ (PDF-651938; a = 4.948 Å; c = 3.977 Å) and $PrNi_5$ (PDF-653469; a = 4.948 Å; c = 3.973 Å).

As compared, the experimental a-cell parameter of $LaNi_5$ is larger than the reference one. The opposite occurs with the c one. The experimental parameters are in good agreement to those reported on high temperature (T > 800 °C) and large annealing time (t > 24 h) samples [10]. The reported cell parameters are a = 5.01 Å; c = 3.98 Å [10]. As observed in Table 1, the a value for $La_{0.25}Ce_{0.52}Nd_{0.17}Pr_{0.06}Ni_5$ is smaller than that of $LaNi_5$ while the c one presents almost no change. This indicates that substitution of lanthanides in the AB_5 structures mostly affects the basal cell parameter.

3.2. Mechanochemical synthesis of $La_{0.25}Ce_{0.52}Nd_{0.17}Pr_{0.06}Ni_5$

3.2.1. Stages of mechanical alloying

The SEM images of starting $LaNi_5$ and $LaNi_5$–$La_{0.25}Ce_{0.52}Nd_{0.17}Pr_{0.06}Ni_5$ mixture are shown in Fig. 3a and b, respectively. $LaNi_5$ shows smooth surfaces with faceted boundaries. Unlike this microstructure, $La_{0.25}Ce_{0.52}Nd_{0.17}Pr_{0.06}Ni_5$ particles in the intermetallics mixture show traces of fracture and cold welding originated during the synthesis method as explained in experimental section. To show the differences, some $LaNi_5$ particles in the intermetallics mixture are indicated with hollow circles and same $La_{0.25}Ce_{0.52}Nd_{0.17}Pr_{0.06}Ni_5$ particles with hollow squares. An example of the binarised (black and white) images used to determine the particle size distribution is presented in Fig. 3c and d, respectively. The mean diameter for $LaNi_5$ is 44 ± 3 μm. The mean diameter for $LaNi_5$–$La_{0.25}Ce_{0.52}Nd_{0.17}Pr_{0.06}Ni_5$ mixture is 10 ± 1 μm, respectively.

As the mixture is milled, the following stages were characterised:

3.2.1.1. Initial stage. Usually, this stage is governed by fracture and milling energy is used to decrease the size of the particles [11,12]. A SEM image of the sample milled for 30 min is shown in Fig. 4a. As observed, the microstructure shows a mixture of particles of each reactant. At this short t_m, the starting reactants are mostly affected by fracture. Nevertheless, the starting morphology of either component in the mixture is still recognised and both $LaNi_5$ and $La_{0.25}Ce_{0.52}Nd_{0.17}Pr_{0.06}Ni_5$ are observed. As an example, some particles of $LaNi_5$ are pointed out with hollow circles and some particles of $La_{0.25}Ce_{0.52}Nd_{0.17}Pr_{0.06}Ni_5$ are identified with hollow squares in Fig. 4a. A diffractogram of the sample milled for 15 min is shown in Fig. 5a (black line). For clarity reasons, only a part of the full diffractogram is shown. The corresponding diffractograms of starting $LaNi_5$ (hollow circles) and starting $La_{0.25}Ce_{0.52}Nd_{0.17}Pr_{0.06}Ni_5$ (full circles) are also shown. Starting AB_5 intermetallics are clearly observed in the sample by analysing the simultaneous presence of the 111 diffraction peaks of $LaNi_5$ and $La_{0.25}Ce_{0.52}Nd_{0.17}Pr_{0.06}Ni_5$ on the as-milled sample (black line). It indicates that chemical composition is not homogeneous in this sample in agreement with *initial stage* of mechanical alloying [11,12]. It must be noticed that compositional changes can not be followed by the analysis of the position of the 002 diffraction peak because both the intermetallics have similar c-cell parameter. This stage is observed up to 30 min.

3.2.1.2. Intermediate stage. This stage is governed by fracture but it is affected by cold welding [11]. The changes on the particle size produced by fracture occur along with the changes of composition due to cold welding [11,12]. A SEM image of a sample milled 75 min is presented in Fig. 4b. It is still observed that the dominant morphology is the one corresponding to the starting particles of $LaNi_5$ (hollow circles). These particles are fractured by processing. Nevertheless, the surface of the larger particles is affected by the welding of the smaller particles of $La_{0.25}Ce_{0.52}Nd_{0.17}Pr_{0.06}Ni_5$. As a result, the particle size is increased slightly reaching values close to 13 μm. The effect of cold welding is observed in the diffractogram of this sample shown in Fig. 5b. The 111 diffraction peak moves to the 2θ values between those of the starting intermetallics. This displacement describes simultaneously the changes in composition related to a and c-cell parameters. In addition, the peaks become broad due to the simultaneous decrease of crystallite size and increase of strain. In this 2θ range of the

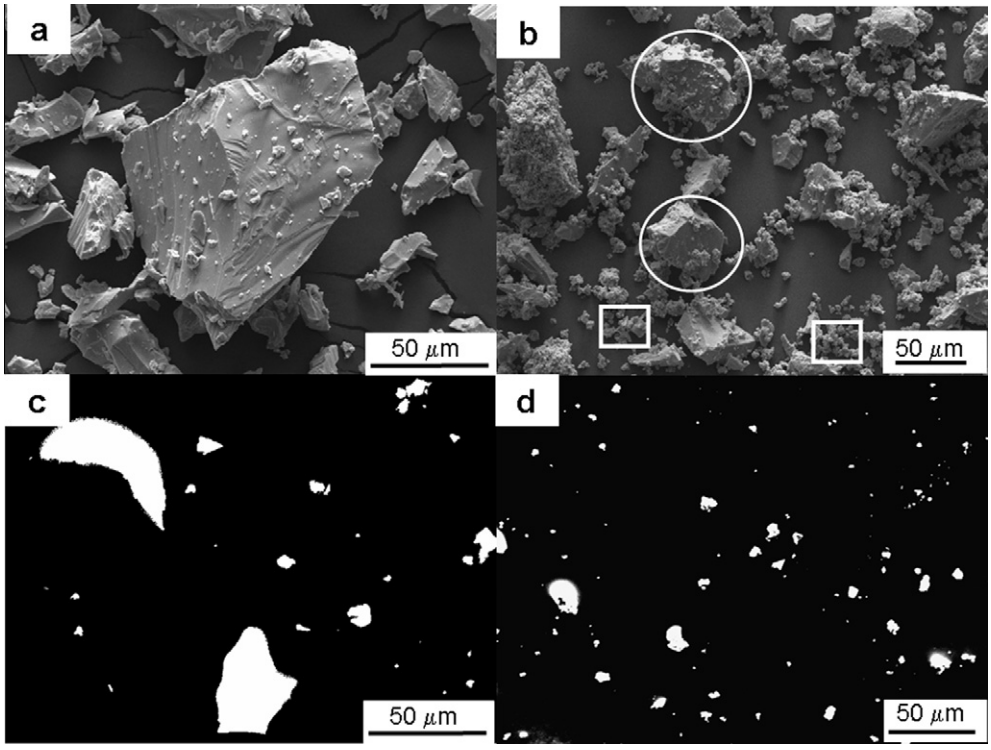

Fig. 3. (a) SEM image of starting $LaNi_5$. (b) SEM image of starting $LaNi_5$–$La_{0.25}Ce_{0.52}Nd_{0.17}Pr_{0.06}Ni_5$ mixture. (c) Example of binarised images (black and white) to determine the particle size distribution of $LaNi_5$. (d) Example of binarised image (black and white) used to determine the particle size distribution of $LaNi_5$–$La_{0.25}Ce_{0.52}Nd_{0.17}Pr_{0.06}Ni_5$.

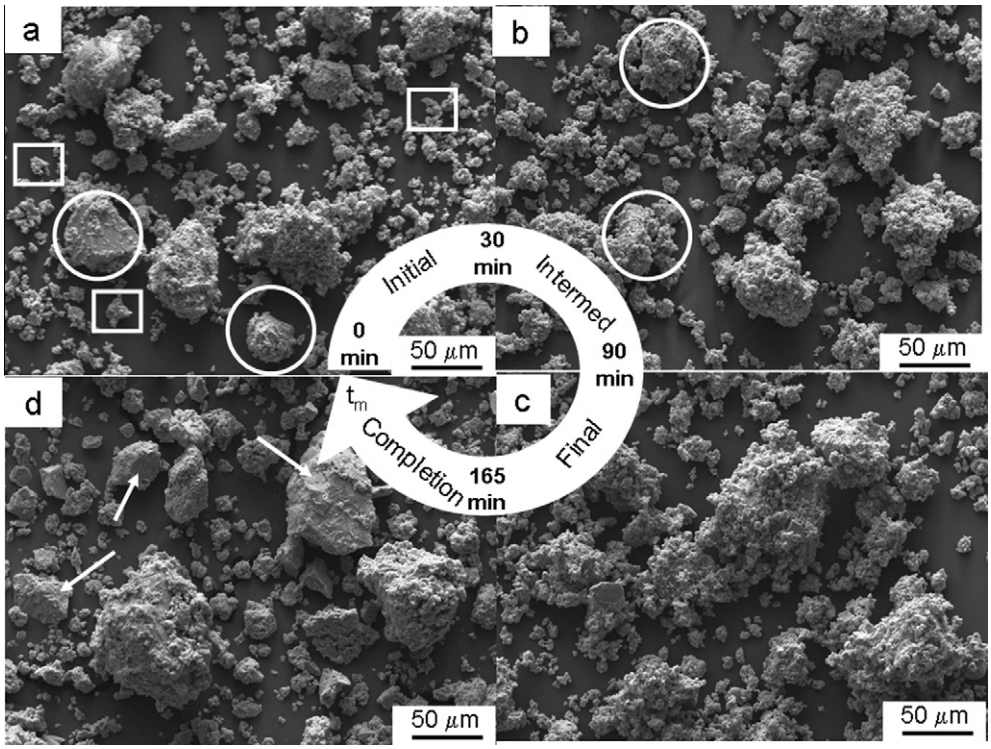

Fig. 4. SEM images of $LaNi_5$–$La_{0.25}Ce_{0.52}Nd_{0.17}Pr_{0.06}Ni_5$ mixture at different stages of milling. (a) *Initial stage*, sample milled 30 min. (b) *Intermediate* stage, sample milled 75 min. (c) *Final* stage, sample milled 165 min. (d) *Completion* stage, sample milled 405 min.

diffractogram, the displacement of the 200 diffraction peak is hidden by the simultaneous broadening of 111 and 200 peaks due to mechanical alloying. On the contrary, the displacement of the 002 diffraction peak position is almost not observed because both $LaNi_5$ and $La_{0.25}Ce_{0.52}Nd_{0.17}Pr_{0.06}Ni_5$ have similar *c*-cell parameter values as shown in Table 1.

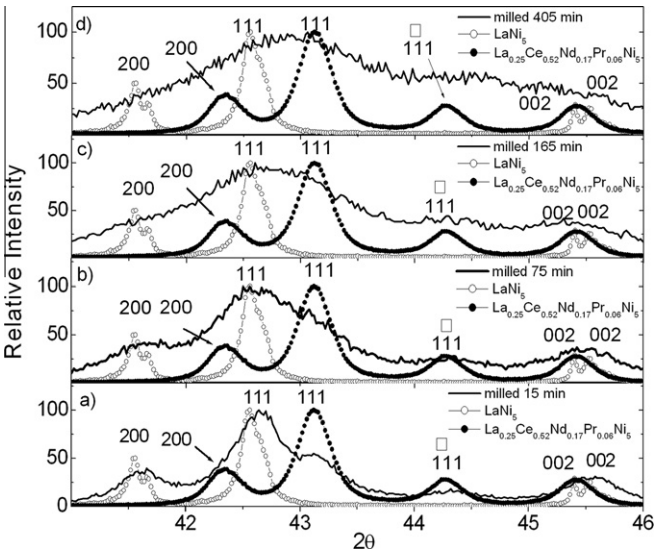

Fig. 5. Diffractogram of samples milled at different t_m (a) 15 min. (b) 75 min. (c) 165 min. (d) 405 min. The diffractograms of starting $LaNi_5$ (hollow circles) and $La_{0.25}Ce_{0.52}Nd_{0.17}Pr_{0.06}Ni_5$ (full circles) are shown for comparison. Ni peaks are labelled with hollow squares.

Table 3
Summary of EDS results in samples as milled 405 min and as milled + annealed. Lanthanides are grouped in A-site of the AB_5.

Particle size (μm × μm)	Atomic percent (±2)				
	La	Ce	Pr	Nd	Ni
As milled sample					
20 × 30	65	22	5	8	5
20 × 30	66	21	4	9	5
10 × 15	67	21	4	8	5
10 × 15	67	21	4	8	5
10 × 15	66	21	4	9	5
Annealed sample					
20 × 30	66	21	4	9	5
20 × 30	66	22	5	8	5
10 × 15	66	21	4	9	5
10 × 15	67	21	4	8	5
10 × 15	66	21	4	9	5

3.2.1.3. Final/completion stages. The final composition is reached at this stage [11,12]. A SEM image of a sample milled 165 min is observed in Fig. 4c. The particles show typical agglomerates produced by the extensive fracture-cold welding combined cycle. A particle size distribution larger than the starting milling times is observed. The corresponding diffractogram is shown in Fig. 5c. The 111 diffraction peak migrates between those of $LaNi_5$ and $La_{0.25}Ce_{0.52}Nd_{0.17}Pr_{0.06}Ni_5$. Table 3 shows EDS measurements for particles milled at this stage. The average composition obtained for this intermetallic is $La_{0.67}Ce_{0.21}Nd_{0.08}Pr_{0.04}Ni_5$. Results are summarised in Table 3. A SEM image of sample milled 405 min is shown in Fig. 4d. The particles show the presence of traces of strong cold welding on the surface (indicated by arrows). The composition does not change as observed in the diffractogram of Fig. 5d. It indicates that the completion stage is reached [11,12].

From these results, the mechanical alloying of the $LaNi_5$–$La_{0.25}Ce_{0.52}Nd_{0.17}Pr_{0.06}Ni_5$ mixture occurs as follows:

Fracture of $LaNi_5$ dominates the *initial* stage ($0\ \text{min} < t_m < 30\ \text{min}$). It occurs because these particles are larger than those of $La_{0.25}Ce_{0.52}Nd_{0.17}Pr_{0.06}Ni_5$. Since both intermetallics have similar ductility, larger $LaNi_5$ particles should be the matrix where $La_{0.25}Ce_{0.52}Nd_{0.17}Pr_{0.06}Ni_5$ particles are welded. As milling progresses, cold welding also influences the process and compositional changes are observed. This stage is denominated as *intermediate* stage and occurs at ($30\ \text{min} < t_m < 90\ \text{min}$). The next stage, denominated as *final* stage is controlled equally by both fracture and cold welding. Final stage occurs for t_m values between 90 and 165 min. At this stage, no further changes on both composition and particle size distribution occur. At longer milling times, *completion* stage occurs. In this particular case the remaining particles show strong effect of the fracture-cold welding cycle.

3.2.2. Characterisation of $La_{0.67}Ce_{0.21}Nd_{0.08}Pr_{0.04}Ni_5$

The diffractogram of the sample milled 405 min is presented in Fig. 5d. The sample was milled enough to reach the *completion* time. Broad diffraction peaks are observed along with the main diffraction peaks of an AB_5 structure. This sample was annealed at 600 °C for 24 h in Ar to increase crystallite size. Therefore, the main and possible minor phases are evidenced. It is presented in Fig. 6. For comparison, the 2θ zones between 42 and 45 of Figs. 5d and 6 should be observed. Three peaks are observed in Fig. 6 in this range while only a broad one is shown in Fig. 5d in the same 2θ range. The final sample presents minor phases. These phases are identified and cell parameters refined. $(La_{0.67}Ce_{0.21}Nd_{0.08}Pr_{0.04})_2Ni_3$ and Ni are the two phases present along the main AB_5 structure. A zoomed zone of the refinement is also presented in the upper inset of Fig. 6. The characteristics and amount of phases present in the final sample are summarised in Table 1. The microstructural parameters were calculated. Summary of results is presented in Table 2.

In Fig. 7, it is shown two SEM images. In Fig. 7a, it is shown the image of a sample milled for 405 min. In Fig 7b, it is shown the image of the corresponding annealed sample. As observed, no morphological changes can be appreciated. The same traces of fracture and cold welding can be identified in both samples. This represents other advantage of this synthesis method because this combined mechanical alloying + low temperature heating increases the grain size but not the particles size.

The effect of grain growth processes increases crystallite size and decreases strain. Results are summarised in Table 2. A summary of EDS measurements done to different particles is presented in Table 3. Lanthanides are grouped in A-site. The average composition obtained corresponds to $La_{0.67}Ce_{0.21}Nd_{0.08}Pr_{0.04}Ni_5$. With in the error of the EDS technique, this value is observed in both as milled and annealed samples. The corresponding EDS plots for a

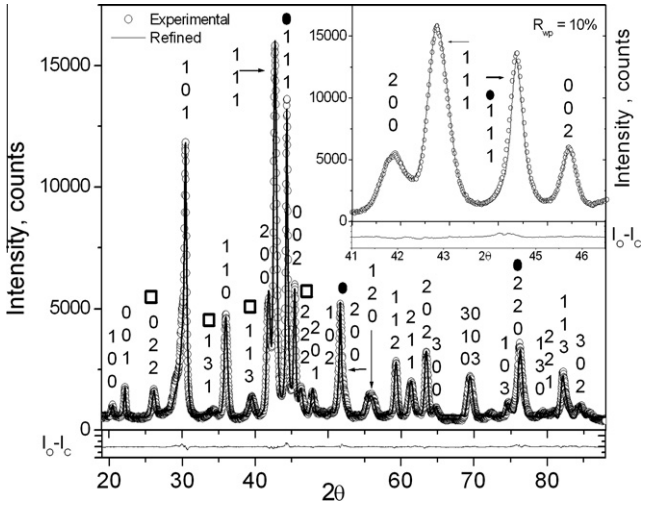

Fig. 6. Diffractogram of annealed $La_{0.67}Ce_{0.21}Nd_{0.08}Pr_{0.04}Ni_5$ sample. Inset: detail of refinement and difference between observed (I_o) and calculated (I_c) intensities. Ni peaks are indicated with full circles. $(La_{0.67}Ce_{0.21}Nd_{0.08}Pr_{0.04})_2Ni_3$ peaks are indicated with hollow squares.

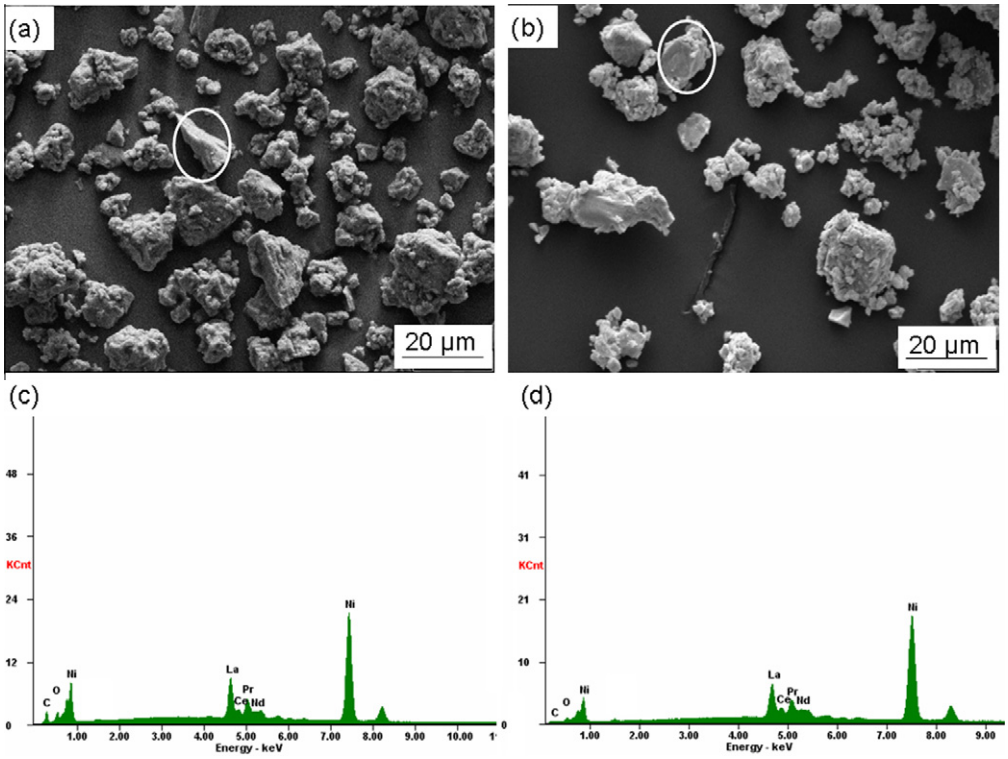

Fig. 7. SEM images. (a) Sample milled for 405 min. (b) Sample as milled for 405 min + annealed at 600 °C for 24 h. The white circle indicates a EDS plot. (c) EDS plot of particle shown in Fig. 7a. (d) EDS plot of particle shown in Fig. 7. b.

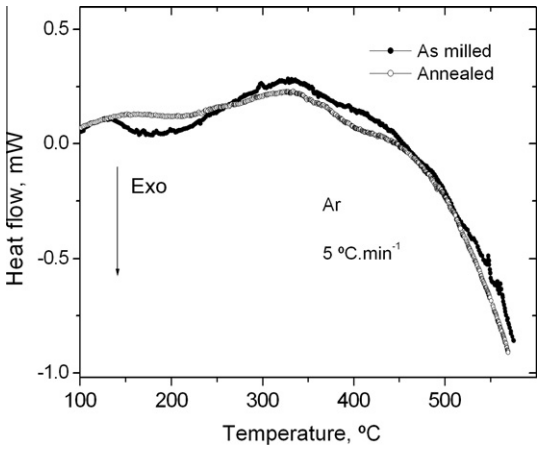

Fig. 8. Calorimetry curves of as-milled and annealed $La_{0.67}Ce_{0.21}Nd_{0.08}Pr_{0.04}Ni_5$ sample.

particle of Fig. 7a and b are shown in Fig. 7c and d, respectively. No marked differences are detected between samples.

The calorimetry curves corresponding to as-milled and annealed samples are presented in Fig. 8. No peaks corresponding to a recrystallization process are observed [13]. It means that only grain growth occurs on the sample. As a result, crystallite size increases and strain decreases. No decomposition peaks are observed. It also indicates that the formation of the secondary phases occurred during the milling process and not because of a destabilization of the main AB_5 phase.

4. Conclusions

The synthesis of $La_{0.67}Ce_{0.21}Nd_{0.08}Pr_{0.04}Ni_5$ was done by mechanical alloying of a $LaNi_5$–$La_{0.25}Ce_{0.52}Nd_{0.17}Pr_{0.06}Ni_5$ mixture. The advantage of using intermetallics instead of metals to obtain the AB_5 is that no preferential lamination of the lanthanide metal on the chamber is observed [4,12]. Therefore, an advance on control of the composition is done. The stages of mechanical alloying were identified and characterised. The *initial* stage occurs from 0 h to 30 min. It is dominated by the fracture of the larger particles of $LaNi_5$. The t_m of this stage can be shortened if $LaNi_5$ is previously milled to reach an average particle size closer to that of $La_{0.25}Ce_{0.52}Nd_{0.17}Pr_{0.06}Ni_5$. *Intermediate* stage occurs from 15 to 90 min. The process is also affected by cold welding inducing compositional changes on the mixture. *Final* stage occurs from 90 to 165 min. Both fracture and cold welding share the control of the process. This t_m is the most relevant data because final composition is reached at this stage. At longer t_m values, *completion* stage occurs. Since *initial* stage is only used to condition the reactants, the effective milling time is only that equivalent to the addition of *intermediate* and *final* stages [12]. This t_m is 150 min. The formation of secondary phases is observed during the process. The secondary phases are homologous to those observed in a typical La-Ni phase diagram.

It is found that *c*-cell parameter in AB_5 structures is almost independent of the lanthanide composition. On the contrary, *a*-cell parameter is found to depend on lanthanide composition. Both parameters influence the volume cell and this last factor is related to the hydrogen sorption properties. The analysis of the hydrogen sorption properties of $La_{0.67}Ce_{0.21}Nd_{0.08}Pr_{0.04}Ni_5$ is the subject of an incoming paper.

Acknowledgements

The authors thank Consejo Nacional de Investigaciones Científicas y Técnicas of Argentina (CONICET) (Project PIP 0109) and Comisión Nacional of Energía Atómica of Argentina (CNEA) for the partial financial support. V. Blanco thank ANPCyT and CNEA for the doctoral Grant (PDFT-PRH-200-4).

References

[1] B.A. Talagañis, M.R. Esquivel, G. Meyer, A two stage compressor based on (La, Ce, Nd, Pr)Ni_5 intermetallics obtained by low energy mechanical alloying – low temperature annealing treatment, Int. J. Hydrogen Energy 34 (2009) 2062–2068.

[2] G. Sandrock, A panoramic overview of hydrogen storage alloys from a gas reaction point of view, J. Alloys Compd. 293–295 (1999) 877–888.

[3] M. Jurczyk, W. Rajewski, W. Majchrzycki, G. Wójcik, Mechanically alloyed $MmNi_5$-type materials for metal hydride electrodes, J. Alloys Compd. 290 (1999) 262–266.

[4] M.R. Esquivel, G. Meyer, A comparison of the evolution during the mechanical alloying of both Mm-Ni and $MmNi_5$-Ni mixtures, J. Alloys Compd. 446–447 (2007) 212–217.

[5] Z. Chen, Z. Chen, Y. Su, M. Lu, D. Zhou, P. Huang, Electrode characteristics of nanocrystalline AB_5 compounds prepared by mechanical alloying, Mat. Res. Bull. 33 (1998) 1449–1455.

[6] C. Lenain, L. Aymard, F. Salver-Disma, J.B. Leriche, Y. Chabre, J.M. Tarascon, Electrochemical properties of AB_5-type-hydride-forming compounds prepared by mechanical alloying, Sol. State Ionics 104 (1997) 237–248.

[7] R.A. Young, A. Sakthivel, T.S. Moss, C.O. Paiva-Santos, DBWS-9411 – an upgrade of the DBWS programs for Rietveld refinement with PC and mainframe computers, J. Appl. Cryst. 28 (1995) 366–367.

[8] R.A. Young, The Rietveld Method, Oxford University Press, Oxford, 1993. pp. 1–53.

[9] A.V. Virkar, A. Raman, Crystal structures of AB_2 and A_2B_7 rare earth-nickel phases, J. Less Common Met. 18 (1969) 59–66.

[10] K. Nassau, L.V. Cherry, W.E. Wallace, Intermetallic compounds between lanthanons and transition metals of the first long period I – preparation, existence and structural studies, J. Phys. Chem. Solids 16 (1960) 123–130.

[11] L. Lu, M.O. Lai, Mechanical Alloying, Kluwer Academic Publishers, Boston, 1998. pp. 69–153.

[12] N.M. Cerón, M.R. Esquivel, Stages of mechanical alloying during the synthesis of Sn-containing AB_5-based intermetallics, Int. J. Hydrogen Energy 35 (2010) 657–662.

[13] J.R. Ares, F. Cuervas, A. Percheron-Guégan, Mechanical milling and subsequent annealing effects on the microstructural and hydrogenation properties of multisubstituted $LaNi_5$ alloy, Acta Mater. 53 (2005) 2157–2167.